On the spatial relationship between auroral electrojets and AE recordings

O.W. Lennartsson
Lockheed Martin Palo Alto Research Laboratory, Palo Alto, CA 94304

March, 1997

Abstract. A recent statistical investigation of the magnetospheric concentration of energetic O^+ ions as a function of the north-south polarity of the interplanetary magnetic field (IMF) has only revealed a rather weak dependence, and it can probably be ascribed to internal magnetospheric substorm processes rather than to a systematic difference in the transmission of solar wind power. This may appear to conflict with the well-known behavior of the auroral electrojet (AE) indices, and raises again the issue of the true meaning of these indices during times of northward IMF, when the northern electrojets are often well poleward of all the AE ground stations. This paper reports on a modest effort to address that issue by using a strongly simplified but globally justifiable system of currents to model the recording of AE indices. It is found that the model can accurately reproduce the average difference in the AE between northward and southward IMF on a geometrical basis, using the same current strength for both IMF polarities. Furthermore, by assuming that the square of the total current is proportional to hourly values of the solar wind kinetic energy flux, using one single proportionality constant and a 1-hour time shift, it is possible to reproduce years of hourly AE values for both IMF polarities, on an average basis.

1. Introduction

As reported in *Lennartsson* [1995], henceforth referred to as Paper I, extensive statistical comparisons between the concentration of energetic (0.1- to 16-keV) O^+ ions in the magnetosphere, including the O^+ energy density, and the concurrent (immediately preceding) interplanetary magnetic field (the IMF) have failed to uncover a direct link betwen the polarity of the IMF B_z (in GSM coordinates) and the O^+ concentration. That is, while the O^+ may increase strongly in numbers during a substorm or a magnetic storm, which is usually preceded by a period of southward IMF B_z, there is no clear evidence that a southward IMF leads to a more efficient direct transfer of solar wind energy to the terrestrial O^+ population than does a northward IMF. The energy density of O^+ ions in the plasma sheet, for instance, as observed from the ISEE 1 spacecraft between 10 and 23 R_E (Paper I), increases with increasing solar wind energy flux (kinetic and electromagnetic alike), wether the IMF is northward or southward, and on a long-term average basis, it is only some 60% larger after a few hours of southward IMF, compared to the same period of northward IMF. That modest difference may well be due to internal "unloading" of stored tail magnetic energy (tail field "dipolarization") during substorms [e.g. *McPherron et al.*, 1973], rather than to increased transmission of external energy across the magntopause.

This property of the O^+ contrasts with the consistently strong response of the auroral electrojet (AE) index to changes in the IMF B_z polarity, as shown by the long-term averages in Table 1. The AE in this table is the present hourly value [*Kamei and Maeda*, 1981, and subsequent data books] at the time of each O^+ sampling, and the IMF B_z is the average hourly value [*Couzens and King*, 1986] during a 3-hour period ending with the second most recent preceding hour, provided that the three consecutive B_z values all had the same sign (see Paper I for details). The more than four-fold increase in the AE from northward to

southward IMF conditions is especially noteworthy since the AE, nominally, is a measure of electric current, via the associated magnetic field, not of the corresponding energy dissipation rate. Assuming that the resistive properties of the ionosphere are the same under both IMF conditions, and that the electrojet strength is a measure of the present level of all dissipating currents, this table implies an 18-fold increase in the energy dissipation rate with a southward IMF, which does not mesh with the barely 60% increase in the O^+ energy density.

Paper I argued that these contrasting attributes of the O^+ population and the AE index probably have more to do with the technique for recording the AE itself than they have with different aspects of the dissipation of solar wind energy, the principal reason being that during times of northward IMF, when the polar caps are contracted, the northern auroral electrojets are typically too far north to produce a meaningful reading of the horizontal magnetic disturbance H at most or all of the 12 existing AE stations. This was substantiated by two independent and complementary computations, namely, on one hand, by statistically correlating the hourly AE with concurrent hourly values of the solar wind energy flux, separately for northward and southward IMF conditions, and, on the other hand, by evaluating the geometrical aspects of a simple line-shaped electrojet at varying geomagnetic latitude. The purpose of this report is to further elaborate on the latter approach, since it turns out to be rather illustrative.

The objectives of the modeling work to be reported here have been the following:

a. The model ought to take into account the most fundamental aspects of high-latitude currents.

b. It should be simple enough to make the results intuitively transparent.

c. It should have the fewest possible free parameters, preferably none.

d. It should only require modest use of a computing facility.

e. In the end, it is only to be applied to a time-averaged AE.

Having any free parameters at all (Objective c) normally implies that there is a particular set of facts, or data points, that a provisional model is meant to reproduce, and that the model itself has some inherent ambiguity in it. That is true to some extent in the present case, as well, but in the end it turns out that the provisional model is able to reproduce a very large set of data, in terms of statistical averaging, with only minor fine-tuning of a single parameter, whose value has been determined a priori, in approximate terms, from a special subset of the data.

2. A Simple Model of AE Recordings

Starting with Objectives b, c and d, the first model of high-latitude currents that comes to mind is made up of line currents. Luckily, this proves to be a rather versatile model, given the relevant circumstances. The specifics are illustrated in Figure 1a, using spherical coordinates r, θ and φ with the polar axis antiparallel to Earth's magnetic dipole, which is assumed centered with its negative end pointing 78.6° N and 70.5° W, in approximate compliance with published coordinates of the AE stations (see below). Furthermore, it is assumed here that the auroral "oval", specifically its equatorward edge, may be well approximated by an offset circle, as discussed by *Holzworth and Meng* [1975], and that the electrojets may be approximated by two half-circular line currents of equal strength at altitude h = 150 km, situated at the equatorward edge and flowing from local noon to local midnight. These electrojets are assumed connected to outer space via two line currents following the shape of dipolar magnetic field lines, $r \propto sin^2\theta$, between the magnetic equatorial plane and, respectively, the noon and midnight points on the oval edge. Panel b of this figure will be described later.

Whether this model also satisfies Objective a is a subtler matter, but Objective e greatly simplifies it. For example, the relative strengths of the two electrojets, although critical to the modeling of the AU and

AL indices separately, is unimportant to a long-term average of the AE index itself, since the AE at any given moment (given minute) is defined by AE = AU - AL, that is essentially by the sum of the two current strengths (*Kamei and Maeda* [1981]; see also *Mayaud* [1980], pp. 96-115, and references therein). For the same reason, it is not important to know exactly where the external field-aligned currents connect to the electrojets in local time, at least not if the lengths of the two electrojets are somewhat comparable on average.

As far as the linear nature of these currents is concerned, there are two mitigating circumstances to keep in mind. One is the considerable distance between these currents and any given point on Earth's surface. At its closest possible approach to one of the "electrojets", that is straight underneath, a ground-based magnetometer would be within a magnetic "footprint" that has a full width at half maximum of no less than 300 km, measured in terms of the standard H component. The other circumstance has to do with Objective e. That is, AE values from different times will necessarily involve measurements made at varying longitudinal distance from the field-aligned currents, because there are only 12 stations, separated by between 4° and 49°, so the (usually minor) contribution to the AE from those currents will, on average, blur the discrete longitude of the source.

The altitude h = 150 km is a rounded and somewhat arbitrary number representing average conditions. The location of true electrojets depends on the altitude distribution of ionospheric conductivity, especially the Hall conductivity, the peak of which varies by several tens of km, depending on varying ionization by solar radiation and auroral electron precipitation [e.g. *Germany et al.*, 1994, and references therein]. It may be argued that the Hall conductivity, as opposed to the Pedersen conductivity, is more typically peaked at 100 km, but for the present modeling, 150 km is a more conservative number, since the main effect to be demonstrated here would be even stronger if the electrojets in Figure 1a were to flow at lower altitude (specific numbers to be given later).

The model neglects the effects of induced currents in Earth's crust (and in electric power lines, oil pipelines, and other manmade structures). These may well be significant in a dynamic situation, when the electrojets are moving rapidly in latitude, for instance, but the induction caused by Earth's slow rotation relative to the external currents is presumably negligible. It also neglects the effects, if any, of having the relative magnetic permeability of Earth's crust be different from unity in the surroundings of each AE station.

Given the radius Θ of the oval, in degrees, and its offset angle δ (assumed strictly anti-sunward here), it is a straightforward task to integrate, numerically, the Biot-Savart Law

$$\mathbf{B}(\mathbf{r}_0) = (\mu_0 / 4\pi) \int I(\mathbf{r})\, \mathbf{dr} \times (\mathbf{r}_0 - \mathbf{r}) / |\mathbf{r}_0 - \mathbf{r}|^3 \qquad (1)$$

along this system of line currents and obtain the magnetic field vector $\mathbf{B}$ at any point $\mathbf{r}_0$ on Earth's surface. To provide a basis for the AE, the magnetic field only needs to be calculated at 12 points, the approximate coordinates of which are listed in Table 2, but the calculations have to be repeated many times during a simulated rotation of Earth in order to yield values representative of long-term averaging.

In order to integrate (1) along the circular portions of the current, it is necessary to express the polar angle θ as a function of the azimuthal angle φ and the two parameters Θ and δ. The exact functional relationship may be obtained from the geometry of oblique spherical triangles [e.g. *Brink*, 1942] via a pair of equations, $tan(90° - \Gamma) = -cos(\varphi) \cdot tan(\delta)$ and $sin(\theta + \Gamma) = cos(\Theta) \cdot sin(\Gamma)/cos(\delta)$, but for the present purpose, sufficient precision is obtained with the computationally simpler planar approximation:

$$\theta \approx \Theta \cdot \sqrt{\{1 - (\delta / \Theta)^2 \cdot (1 - cos^2(\varphi))\}} - \delta \cdot cos(\varphi) \qquad (2)$$

The radius Θ is related to the IMF B_z, in units of nT, via the least-squares fit in Figure 3 of *Holzworth*

and Meng [1975]:

$$\Theta \approx 18.9° - 0.919\, B_z \qquad (3)$$

This linear relationship (inferred from a graph) was derived by those authors from 15 events, with B_z having values between about -4.5 and +3.5 nT, and it may not be valid for much larger absolute values. Therefore, the present modeling has been limited to solar wind conditions with -5 nT $\le B_z \le$ 5 nT.

An approximate offset angle δ may be inferred from the quantity A_2 in Table 1 of Holzworth and Meng as a function of the geomagnetic activity index Q, but to simplify matters here, only two values are used, namely 3° for northward IMF, which typically corresponds to "weak activity", and 5° for southward IMF, or "enhanced activity". Although B_z values near zero are not actually used below, the formal rule is thus:

$$\delta = 3° \text{ for } B_z \ge 0 \qquad (4a)$$
$$\delta = 5° \text{ for } B_z < 0 \qquad (4b)$$

The only remaining free parameter is now the total current strength I; otherwise the model is set up for deriving the magnetic field at any of the AE stations, given the rotational phase of Earth as a function of time. In analogy with the real process of obtaining one-minute AE values [*Mayaud*, 1980; *Kamei and Maeda*, 1981], only the locally horizontal and northward component H (opposite the θ unit vector here) of the disturbance field is considered, and the AE, accordingly, is calculated as the difference between the uppermost value of H recorded at any of the 12 stations in a given minute, the AU, and the lowermost value of H recorded at any of the other 11 stations in the same minute, the AL, sign included. Because of the 11.4° tilt of the dipole, each successive minute of Universal Time (UT) corresponds to a (slightly) varying increment of the magnetic longitude angle φ_0 of a given station, counted positive eastward from local noon, in accordance with Figure 1a. Specifically, if t is the UT in minutes and $\omega t = 0.25t$ (ω in degrees per minute) is the geografic local time angle of the Greenwich meridian, then:

$$cos(\varphi_0(t) - \varphi_0') = -cos(\omega t - 70.5°) / \sqrt{\{1 - sin^2 11.4° \cdot sin^2(\omega t - 70.5°)\}} \qquad (5)$$

where φ_0' is the fixed longitude angle of the station from Table 2, and 70.5° is the west geographic longitude of the North Magnetic Pole.

2.1. Numerical Evaluation

Figure 2 shows 24-hour time series of simulated AU (top panel), AL (middle panel) and AE (bottom panel), assuming a constant total current of 10^6 A, that is 500 kA in each electrojet, and a constant IMF with a z-component of either +5 nT (northward; dotted lines) or -5 nT (southward; solid lines).

The feature of special significance here is the low strength of the indices for northward IMF. This is a consequence of two conspiring effects, namely (*i*) the large distance of most AE stations from the electrojets, which affects the absolute magnitude of the local magnetic field, and (*ii*) the small elevation angle of the electrojets above the horizon, which makes the measured H component a small part of the total field. This feature would still be present if the currents had finite thickness, and would be still more pronounced if the electrojets were to extend a substantial distance poleward of the oval edge, further away from the AE stations. Having the electrojets at lower altitude, at 100 km, say, would slightly increase these indices, because of the reduced distance, but the smaller elevation angle would make the difference between northward and southward IMF stronger (see below). The enhanced strength shown by the dotted lines at the beginning of the day, and toward the end, is due mainly to one single AE station, namely the geomagneti-

cally northernmost station, Narssarssuaq in Greenland (IAGA abbrev. NAQ; the leftmost in Table 2).

For southward IMF the indices are much stronger but also greately varying, due to the wide longitudinal gaps between most of the stations. The strongest H component from a 500 kA line current at 150 km altitude is about ± 667 nT, straight underneath the current, which is reached by most of the peaks in, respectively, the AU and AL indices. The various peaks reflect the successive re-assignment of the AU and AL indices to the two stations with the current extreme positive and negative H. When averaged over the entire 24-hour day, these AU and AL are, respectively, about 406 nT and -446 nT. The corresponding 24-hour AE is, of course, 852 nT, and that is roughly ten times greater than the 24-hour AE for northward IMF (about 80 nT).

The jagged appearance of these indices for southward IMF could be smoothed by giving the electrojets a finite cross section, at great cost in computing time, but making them merely a few hundred km wide in latitude would not have a large effect, being that they are at 150 km altitude. For a crude illustration of the latter, see Figure 3.

To calculate the AE in Figure 3, the single current system in Figure 1a has been replaced by three systems of the same type, all with their electrojets at the same altitude and with the same offset angle δ, but separated in their radial extent by 1° (about 114 km) and each carrying part of the same total current I. The middle system has its electrojets at the radius Θ, as defined by (3), and carries half the total current ($I/4$ in each electrojet); the adjacent systems have their electrojets at radii $\Theta \pm 1°$, respectively, and carry one fourth of the total current each ($I/8$ per electrojet). The resulting AE is somewhat smoother than in Figure 2, but not necessarily more "realistic", since all currents are at the same altitude.

The 24-hour average AE in Figure 3 is 90 nT for northward IMF and about nine times greater, 779 nT, for southward IMF. Hence, spreading the electrojet current over latitude alone does tend to reduce the large difference between northward and southward IMF in the AE, but that effect is partially counteracted if the current, at the same time, is also spread over altitude (not shown). Adding many more such partial current systems, using not only different Θ and h, but also different values for δ and for the longitudes of the field-aligned currents, could approximate finite cross section currents with ever improving accuracy, but this approach would add any number of free parameters to be matched to data, a sharp departure from Objective c in the Introduction.

The fundamental cause of the large time variations in these simulated indices for southward IMF is the finite offset angle δ, which makes it posible for AE stations to cross underneath the model electrojets. If this angle is set to zero (not shown), while B_z and I are kept the same, the AU and AL become almost constant with, for southward IMF and one single current system as of Figure 1a, a magnitude between about 600 nT and 667 nT, except for a brief dip to 350 nT at about 05 UT in the AU and about 17 UT in the AL (12 hours later). The AE, of course, is about twice as strong with two dips to about 950 nT. More significantly, perhaps, all indices become even weaker than they are in Figure 2 for northward IMF.

A contributing factor, although a minor one, to the weak indices for northward IMF is the H component from the field-alignet portions of the current, which has a direction opposite the H component from the electrojets at ground level. For southward IMF, when the polar cap is large, the latter is strongly dominant in the indices (which are from stations close to the electrojets), but as the polar cap contracts, for northward IMF, the H component from the electrojets decays faster than that from the field-aligned currents, for geometrical reasons, leaving the field-aligned currents with a relatively stronger influence. This can be made more tangible by calculating the AE indices from the current system in Figure 1b.

The closed-loop currents in Figure 1b (still assuming h = 150 km) can be envisioned, very crudely, as pure Hall currents, flowing antiparallel to the high-latitude $\mathbf{E}\times\mathbf{B}$ drift (carried by the electrons who have a larger average drift speed than the ions at these altitudes). That is, the single cross-polar current I is to be associated with the anti-sunward polar cap convection, and the electrojets with the sunward convection at lower latitude. Superficially, at least, it seems possible that the net magnetic field at ground level is mainly due to such closed current loops within the ionosphere itself. This topic will be revisited briefly in the conclusion section below. In any case, it is illustrative to calculate the corresponding AE index, and the

result is shown in Figure 4.

The AE in Figure 4 is consistently larger than in the bottom panel of Figure 2, although that is hard to tell visually for southward IMF (solid line). The reason it is larger is that the cross-polar current I is mostly "out of sight", in terms of its H component, from all AE stations, in contrast to the field-aligned currents in Figure 1a. During the 24-hour rotation of Earth, most AE stations do pass underneath this current for southward IMF, but at those times the associated magnetic field at ground level points mostly in the longitudinal direction and does not contribute a great deal to the meridional H component. For northward IMF (dotted line) the absence of field-aligned currents is somewhat more noticeable, at least early in the day and near the end.

Of the two current systems in Figure 1, the one with external field-aligned "supply" currents in Panel a has proved to be the better model when it comes to reproducing the observed difference between northward and southward IMF in the time-averaged AE index. The system in Panel b can be improved upon in this regard (not shown) by dividing the single cross-polar current I into two separate currents $I/2$ flowing on either side of the magnetic pole, at some distance from the pole, and shortening each electrojet correspondingly, but that modification requires at least one additional free parameter, and that again defeats Objective c in the Introduction. Therefore, only the model in Panel a is used below, and only one at a time.

3. Applying the Model to Statistical Results From O^+ Study

The average AE values in Table 1 emerged as by-products from a combined filtering of IMF conditions and magnetotail plasma properties (Paper I) with no restriction on universal time. Indeed, each of the two AE numbers in this table is based on a virtually random sampling of the hour of the day. To apply the present model to these numbers it is thus appropriate to average all one-minute values into a single 24-hour average AE for a given set of I, Θ, and δ. The oval radius Θ is defined from B_z in Table 1 via equation (3), and δ follows from equations (4a) or (4b). Because equation (1) is linear in I, it is a simple matter to infer the optimal value of this, as of now, free parameter by linear extrapolation from a single trial value.

By choosing $I = 510573$ A it is possible to reproduce the AE in Table 1 for southward IMF with better than 0.1 nT precision, as shown in Table 3. As this table also shows, the very same value of I reproduces the average AE for northward IMF with better than 1 nT precision. This is probably a fortuitous coincidence, considering the simplistic nature of the model, but it does seem to confirm the presumption in Paper I that the typical difference between hourly AE values recorded during times of different polarity of the IMF B_z has more to do with the location of the electrojets than it has with their strength.

4. Removing the Last Free Parameter

The statistical correlations made in Paper I between the hourly AE and hourly representations of the recent solar wind energy flux, treating the kinetic flux K and the electromagnetic (Poynting) flux P along the solar wind flow vector separately, revealed two major features: (*i*) The degree of correlation is best with a time shift of less than two hours between the energy flux input and the AE output, and marginally better with a one-hour shift than with no shift. (*ii*) The AE on average is nearly proportional to the square root of K (but not to the square root of P), with different proportionality factors for northward and southward IMF. It was surmised that the true relationship is indeed proportionality, and that the two factors would become equal if the AE were "corrected" for the varying latitude of the electrojets.

The present model provides a means to test that kind of dependence of AE on K indirectly, by calculating

simulated indices that do take the geographical (i.e. geometrical) relationships into account, albeit in a strongly simplified fashion. The key parameter for that is the total current strength I, which is thus to be assumed proportional to $K^{1/2}$, leaving the constant proportionality factor as the last "free parameter" of the model. This parameter is actually free only in a very limited sense by now, because Table 3 defines an average current density for the times included in the O^+ study, and this current density ought to be somewhat consistent with the corresponding measured averages of $K^{1/2}$, even though the solar wind conditions in that case refer as far back as 2-4 hours earlier (see comments on Table 1 above). The result of that comparison (details not shown here), expressed in terms of the energetically more appropriate form of I^2, is

$$I^2 \approx (5.1 \pm 0.2)\ 10^{14}\ K \qquad (6)$$

The purpose of the following statistical application of the model is two-fold, namely (*i*) to demonstrate that this type of relationship can reproduce the actual hourly AE on a larger scale than that defined by the O^+ study and (*ii*) to suggest a more precise value for the proportionality constant. Having hourly values as the basic granularity for AE justifies using the convenient electronic OMNI file [*Couzens and King*, 1986] to obtain hourly representations of K as well, assuming a flowing Maxwell-Boltzmann distribution,

$$K = n\, m\, |\mathbf{v}|^3 /2 + 5\, n\, k\, T\, |\mathbf{v}| /2 \qquad (7)$$

by inserting the hourly proton density n, bulk flow velocity $\mathbf{v}$ (modified to include Earth's orbital motion), and thermal energy kT listed in that file (m is the proton mass). In accordance with Objective e in the Introduction, the simulated AE does not have to agree closely with the actual index on an hour-by-hour basis, but the model ought to capture the "average dependence" of AE on K and, in particular, on the polarity of the IMF B_z.

In order to apply the model to a large set of hourly B_z and K it is, however, necessary to impose certain restrictions on B_z. As already mentioned, the least-squares fit (3) for Θ may not hold for $|B_z| > 5$ nT, and hourly values of B_z near zero do not necessarily have a physically meaningful polarity. As a conservative measure, $|B_z|$ has been limited to 3-5 nT here, thus defining two distinctly separate sets of northward and southward IMF. This limitation also avoids possible problems with the discontinuity in the offset angle δ at zero B_z, as imposed by (4a) and (4b).

The individual numbers used for B_z (also from *Couzens and King* [1986]), as well as those used for K, are from the UT hour immediately preceding the time tag of I, so as to replicate the optimal one-hour shift found in Paper I in the correlation between solar wind energy flux and the real hourly AE index. If, finally, the approximation (6) is replaced by the following more specific relationship between I (A) and K (W/m^2),

$$I^2 = 5.16\ 10^{14}\ K \qquad (8)$$

and the model is applied to all (suitable) solar wind data from the January 1, 1978, through March 1, 1980, period (same span as in Table 1, but much denser coverage), the results are as listed in Table 4.

In this case the simulated AE has been calculated only once each UT hour, with Earth's position determined at the 30-minute mark, both because a minute-by-minute calculation would have required a rather substantial computation time (several hours with the available equipment), and because there is only a single set of B_z and K available for each hour. This simplification is not believed to have produced a systematic bias, but it has probably contributed some part of the scatter in the simulated hourly values. The error margins shown, in both the simulated and the real AE, are the one sigma uncertainty in the average itself, which is equal to the sample standard deviation divided by the square root of the number of samplings (hours). The simulated and real AE do not always agree well on an hour-by-hour basis, but considering the

very large number of samplings, the correlation is on the whole quite good, with a correlation coefficient of 0.15 for northward and 0.36 for southward IMF. The statistical spread, due in large part to the spread in the solar wind inputs, is also similar for both kinds of AE, as reflected by Table 4.

5. Concluding Remarks

The essential lesson to be learned from this numerical exercise is that the typical difference between an AE index, at least an hourly AE, obtained while the IMF is northward, and another obtained while the IMF is southward, can probably be accounted for by geometrical considerations, even quantitatively. There is no obvious need, based on the AE alone, to postulate a systematic difference in the rate of transfer of solar wind energy to the corresponding high-latitude currents.

The fact that equation (8) is able to reproduce the real average AE in Table 4 with both northward and southward IMF is significant but not essential; other assumed forms of solar wind control of the current strength may produce similar results, as long as the current is suitably normalized and, on average, approximately equal for northward and southward IMF (cf. Table 3). Although (8) is reminiscent of a power conversion formula, the main impetus for using it here is that it may explain the statistical correlation of the real hourly AE with concurrent hourly values of K, as surmised in Paper I. To the extent that real electrojets are carried by a Hall current, they flow perpendicularly to the local electric field and thus are actually dissipation-free. The electric dissipation of solar wind power must be brought about by the associated Pedersen current, and by systems of field-aligned current, including the large east-west oriented sheets of opposing "Region 1 and 2 currents" [e.g. *Iijima and Potemra*, 1976]. The geometry of those currents may be such as to produce a relatively weak net magnetic field at ground level, as compared to the field from the Hall current, especially in terms of the H component. The result reached in Table 4 may reflect that the Hall current, on average, is proportional to the other currents.

The simplistic system of line currents in Figure 1a is far from "realistic" in a literal sense, but the odds are that it does capture the significant geometry on a global scale. The most obvious point in its favor is that it can be made to reproduce, virtually "exactly", the observed dependence of the AE on the IMF north-south polarity by assigning the same constant value to a single parameter, such as the proportionality constant in (8), for both polarities. Spreading the electrojet current across several degrees of latitude would have the effect of reducing, to some extent, the difference in the AE between northward and southward IMF, as suggested by the above results with multiple line currents (Figure 3), but there are additional justifiable "improvements" that would have the opposite effect. One is to also spread the electrojet current across a range of altitude (not shown), another is to reduce the altitude of that current as a whole to make it agree somewhat better with the distribution of the Hall conductivity [e.g. *Germany et al.*, 1994]. For example, if the model electrojets in Figure 1a are lowered from h = 150 km to h = 100 km, and the constant in (8) is adjusted (reduced) to still produce an average AE of 405 nT for southward IMF, as in Table 4, then the average AE for northward IMF is reduced from 89 to 82 nT.

These geometrical aspects have potentially important implications for one's interpretation of variations in the AE index, even on a scale of minutes. As a minimum, they suggest a simple explanation for the very good correlation that has been found between the AE and the equatorward displacement of the auroral oval [e.g. *Eather et al.*, 1979, and references therein]. Furthermore, consider the simulated 1-minute AE in Figure 2, for instance. If the IMF B_z were to suddenly change from + 5 nT to - 5 nT around 1500 UT, say, it is easy to envision that the AE would increase from about 50 nT to more than 1200 nT over the course of probably less than an hour, without the currents having to actually change in magnitude. A response time of less than an hour for the auroral oval to increase its radius from 14.3° to 23.5°, in accordance with the empirical relation (3) above, that is an expansion rate of a little more than 0.15° per minute, is well within

the limits suggested by all-sky photographic records [e.g. *Cresswell*, 1968; *Eather et al.*, 1979]. The associated increase in the AE would undoubtedly qualify as a substorm "growth phase" in standard nomenclature [e.g. *McPherron et al.*, 1973], and yet it might not involve an increased input of solar wind power, unless, of course, the reversal of the IMF B_z is spatially associated with a solar wind shock front, in which case K would increase in (8).

Generally speaking, however, the implications are that the typically rapid and large, often "spike-like", fluctuations in the AE during substorms (see for example the 1-min plots in *Kamei and Maeda* [1981]) cannot be presumed to track the variations in the solar wind power input, or track the "unloading" of tail magnetic energy [*McPherron et al.*, 1973], for that matter; they may have as much or more to do with rapid motion of the electrojets back and forth across the AE stations.

Acknowledgments. Magnetic tape records of geomagnetic indices and of solar wind particle and interplanetary magnetic field data were provided by, respectively, NOAA and NSSDC. This work was supported by NASA under contract NASW-4816.

References

Brink, R.W., *Spherical Trigonometry*, Appleton-Century-Croft, Inc., New York, 1942.

Couzens, D.A., and J.H. King, *Interplanetary Medium Data Book, Supplement 3, 1977-1985*, Rep. NSSDC /WDC-A-R&S 86-04, NASA Goddard Space Flight Cent., Greenbelt, Md., 1986.

Cresswell, G.R., Fast auroral waves, *Planet. Space Sci., 16,* 1453, 1968.

Eather, R.H., S.B. Mende, and E.J. Weber, Dayside aurora and relevance to substorm current systems and dayside merging, *J. Geophys. Res., 84,* 3339, 1979.

Germany, G.A., D.G. Torr, P.G. Richards, M.R. Torr, and S. John, Determination of ionospheric conductivities from FUV auroral emissions, *J. Geophys. Res., 99,* 23297, 1994.

Holzworth, R.H., and C.-I. Meng, Mathematical representation of the auroral oval, *Geophys. Res. Lett., 2,* 377, 1975.

Iijima, T., and T.A. Potemra, The amplitude distribution of field-aligned currents at northern high latitudes observed by Triad, *J. Geophys. Res., 81,* 2165, 1976.

Kamei, T., and H. Maeda, Auroral electrojet indices (AE) for January-June 1978, *Data Book No. 3*, World Data Center C2 for Geomagn., Kyoto, Japan, 1981.

Lennartsson, O.W., Statistical investigation of IMF B_z effects on energetic (0.1- to 16-keV) magnetospheric O^+ ions, *J. Geophys. Res., 100*, 23621, 1995.

Mayaud, P.N., *Derivation, Meaning, and Use of Geomagnetic Indices,* American Geophysical Union, Geophysical Monograph 22, Washington, D.C., 1980.

McPherron, R.L., C.T. Russell, and M.P. Aubry, Satellite studies of magnetospheric substorms on August 15, 1968, 9, Phenomenological model for substorms, *J. Geophys. Res., 78,* 3131, 1973.

O.W. Lennartsson, Lockheed Martin Palo Alto Research Laboratory,
Org. H1-11, Building 252, 3251 Hanover Street, Palo Alto, CA 94304.
(e-mail: lenn@space.lockheed.com)

Table 1. Averages From a Study of Oxygen Ions in the Central Plasma Sheet (Jan 1, 1978 - Mar 1, 1980)

	O^+ Energy Density (eV/cm^3)	Preceding IMF B_z (nT)	Current AE (nT)
Northward IMF	128	+ 3.7	97
Southward IMF	200	- 3.4	413

Table 2. Geomagnetic Latitudes and Longitudes of the 12 AE Stations (from *Kamei and Maeda*, 1981)

Lat (°N)	71.2	70.2	66.0	63.0	66.3	60.4	61.8	68.5	64.6	69.0	68.7	66.6
Lon (°E)	36.8	71.0	115.1	161.6	176.5	191.4	237.1	241.2	256.5	292.8	322.8	347.4

Table 3. 24-Hour Average AE With Current I = 510573 A Flowing at Two Different Locations

	Circle Radius Θ	Circle Offset δ	Simulated Average AE (nT)
Northward IMF	15.5°	3.0°	96.5
Southward IMF	22.0°	5.0°	413.0

Table 4. 26-Month Average AE (nT). Includes 1409 Hours For Northward IMF, 1560 For Southward IMF

	Allowed Range of B_z	Offset δ	Simulated AE	Real AE
Northward IMF	+3 nT ≤ B_z ≤ +5 nT	3°	89 ± 3	91 ± 3
Southward IMF	-5 nT ≤ B_z ≤ -3 nT	5°	405 ± 5	404 ± 5

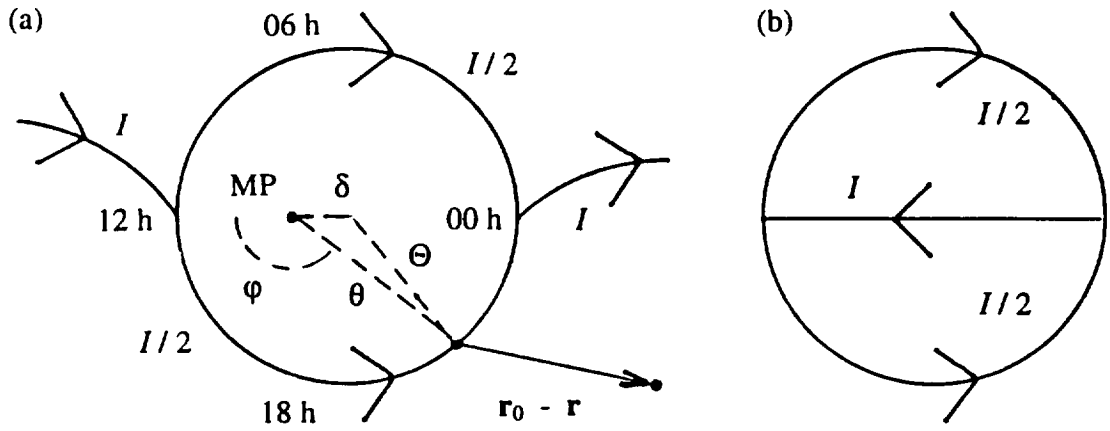

Figure 1. (a) Line model of high-latitude currents. Circular portion follows equatorward edge of auroral oval, at altitude h = 150 km. Oval center is offset from magnetic pole (MP) by δ degrees toward local midnight. Connecting currents follow magnetic dipole field lines (see text). Point $\mathbf{r}_0$ (magnetometer) is on Earth's surface. (b) Alternative (closed-loop) currents at constant altitude h.

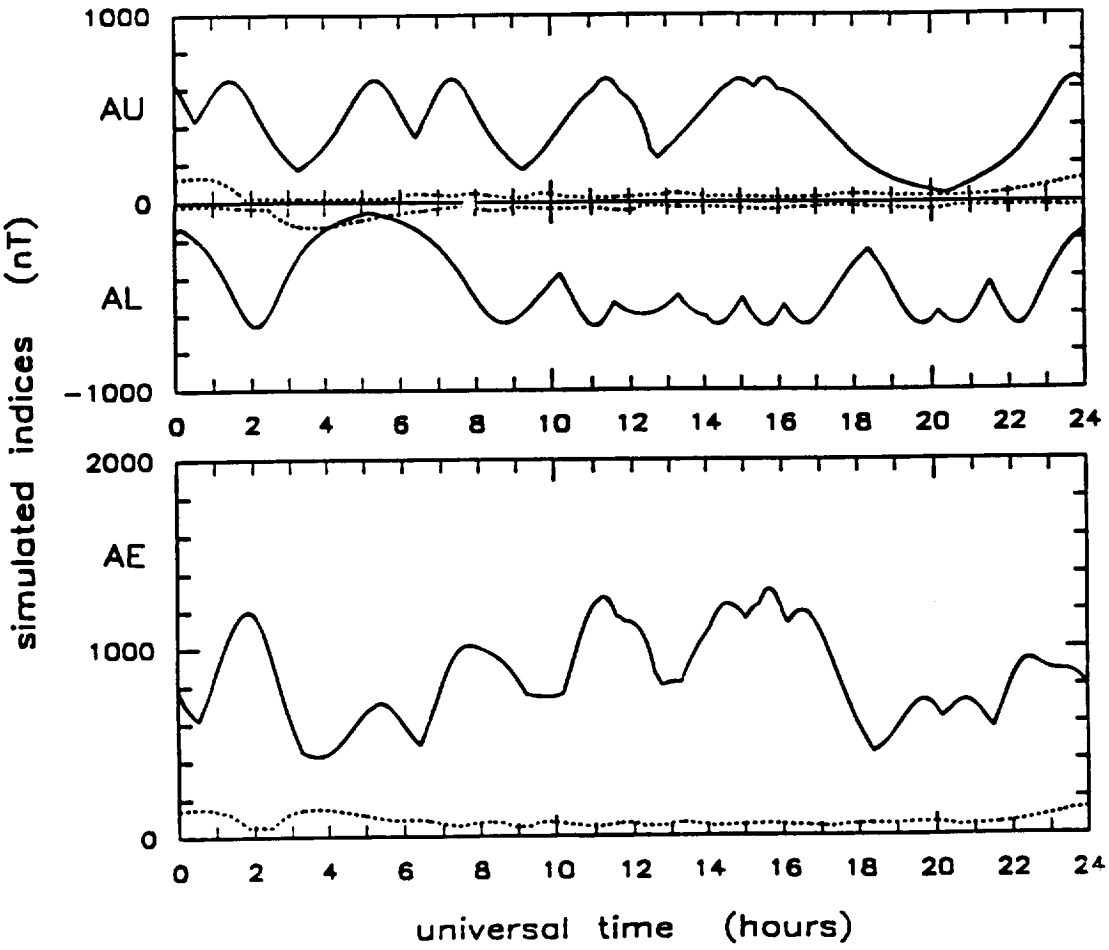

Figure 2. Simulated 1-minute (top) AU, (middle) AL, and (bottom) AE = AU - AL with I = 1 MA and IMF B_z = +5 nT (dotted lines) and = -5 nT (solid lines). Current system as defined in Figure 1a.

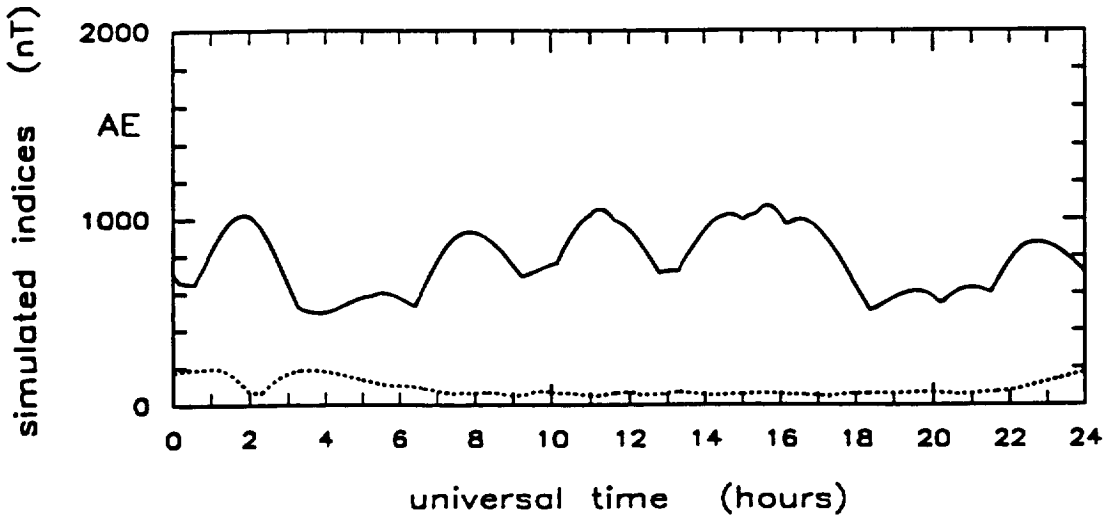

Figure 3. Same as bottom panel of Figure 2 but subdividing the current into three systems of the type defined in Figure 1a, all with h = 150 km and separated from each other by 1° in radius Θ (see text).

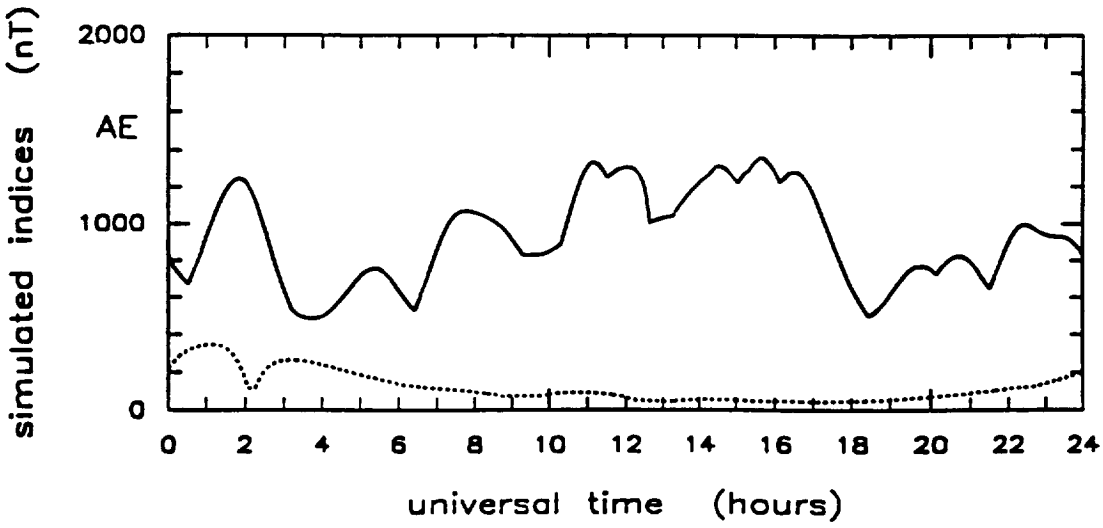

Figure 4. Same as bottom panel of Figure 2 but using current system as defined in Figure 1b.